HAL
open science

A Reversible Phase Transition for Sodium Insertion in Anatase TiO 2

Wei Li, Mika Fukunishi, Benjamin. J. Morgan, Olaf J. Borkiewicz, Karena W. Chapman, Valérie Pralong, Antoine Maignan, Oleg I. Lebedev, Jiwei Ma, Henri Groult, et al.

To cite this version:

Wei Li, Mika Fukunishi, Benjamin. J. Morgan, Olaf J. Borkiewicz, Karena W. Chapman, et al.. A Reversible Phase Transition for Sodium Insertion in Anatase TiO 2. Chemistry of Materials, 2017, 29 (4), pp.1836-1844. 10.1021/acs.chemmater.7b00098 . hal-01472355

HAL Id: hal-01472355

https://hal.sorbonne-universite.fr/hal-01472355v1

Submitted on 20 Feb 2017

HAL is a multi-disciplinary open access archive for the deposit and dissemination of scientific research documents, whether they are published or not. The documents may come from teaching and research institutions in France or abroad, or from public or private research centers.

L'archive ouverte pluridisciplinaire **HAL**, est destinée au dépôt et à la diffusion de documents scientifiques de niveau recherche, publiés ou non, émanant des établissements d'enseignement et de recherche français ou étrangers, des laboratoires publics ou privés.

A Reversible Phase Transition for Sodium Insertion in Anatase TiO_2

Wei Li,[†] Mika Fukunishi,[§] Benjamin. J. Morgan,[‡] Olaf J. Borkiewicz,[⊥] Karena W. Chapman,[⊥] Valérie Pralong,[°] Antoine Maignan,[°] Oleg I. Lebedev,[°] Jiwei Ma,[†] Henri Groult,[†] Shinichi Komaba,[§] Damien Dambournet[†,][||,*]

† Sorbonne Universités, UPMC Univ Paris 06, CNRS UMR 8234, Laboratoire PHENIX, 4 place Jussieu, F-75005 Paris, France.

§ Department of Applied Chemistry, Tokyo University of Science, 1-3 Kagurazaka, Shinjuku, Tokyo 162-8601, Japan.

‡ Department of Chemistry, University of Bath, Claverton Down, BA2 7AY, United Kingdom.

⊥ X-ray Science Division, Advanced Photon Source, Argonne National Laboratory, 9700 South Cass Avenue, Argonne, Illinois 60439, United States.

° Laboratoire CRISMAT, ENSICAEN, Université de Caen, CNRS, 6 Bd Maréchal Juin, F-14050 Caen, France.

[] Réseau sur le Stockage Electrochimique de l'Energie (RS2E), FR CNRS 3459, France.

ABSTRACT: Anatase TiO_2 is a potential negative electrode for sodium-ion batteries. The sodium storage mechanism is, however, still under debate, yet its comprehension is required to optimize the electrochemical properties. To clarify the sodium storage mechanism occurring in anatase, we have used both electrochemical and chemical routes from which we obtained similar trends. During the first discharge, an irreversible plateau region is observed which corresponds to the insertion of Na^+ within the interstitial sites of anatase and is accompanied by a drastic loss of the long-range order as revealed by x-ray diffraction, high resolution of high angle annular dark field scanning transmission electron microscope (HAADF-STEM) and pair distribution function (PDF) analysis. Further structural analysis of the total scattering data indicates that the sodiated phase displays a layered-like rhombohedral R-3m structure built from the stacking of Ti and Na slabs. Because of the initial 3D network of anatase, the reduced phase shows strong disorder due to cationic inter-mixing between the Ti and Na slabs and the refined chemical formula is $(Na_{0.43}Ti_{0.57})_{3a}(\square_{0.22}Na_{0.39}Ti_{0.39})_{3b}O_2$ where $\square$ refers to vacancy. The presence of high valence Ti ions in the Na layers induces a contraction of the *c*-parameter as compared to the ordered phase. Upon de-sodiation, the structure further amorphized and the local structure probed by PDF is shown to be similar to the anatase TiO_2 suggesting that the 3D network is recovered. The reversible sodium insertion/de-insertion is thus attributed to the rhombohedral active phase formed during the first discharge, and an oxidized phase featuring the local structure of anatase. Due to the amorphous nature of the two phases, the potential-composition curves are characterized by a sloping curve. Finally, a comparison between the intercalation of lithium and sodium into anatase TiO_2 performed by DFT calculations confirmed that for the sodiated phase, the rhombohedral structure is more stable than the tetragonal phase observed during the lithiation of nanoparticles.

Introduction

In many areas of modern life, lithium-ion batteries are ubiquitous as energy-storage solutions. The growing demand for higher energy density and lower cost of electrochemical energy storage devices, however, has motivated a search for auxiliary technologies based on alternative chemistries.[1,2] One possible candidate is the sodium-ion battery, which is attractive because of the high earth–abundance of sodium, and lower cost versus lithium-ion batteries, due to compatibility with aluminum as the anodic current collector.[3-5] Development of sodium-ion batteries has been largely stimulated by knowledge of lithium-ion analogues. The intercalation of Na^+ or Li^+ ions into a host lattice can, however, give qualitatively different voltage profiles, corresponding to different intercalation mechanisms. For example, lithium insertion in $Li_4Ti_5O_{12}$ is accompanied by a spinel to rock-salt phase transition. [6,7] The equivalent sodium insertion, however, proceeds via a complex three-phase–separation mechanism (spinel to two rock-salt phases of $Li_7Ti_5O_{12}$ and $Na_6LiTi_5O_{12}$).[8] Such differences in intercalation behaviour can often be attributed to different properties of Li versus Na, such as ionic radius and polarizability.[9, 10] In general, however, the performance of electrodes in sodium-ion batteries cannot be understood by simply extrapolating from their behaviour versus lithium, when it is necessary to carefully reexamine the sodium-intercalation behaviour.

In the search for new sodium-ion anodes, many titanium-based compounds, with diverse structures and chemistries, have been considered. These include titanium sulfate,[11] phosphate,[12] sodium/lithium titanate,[6,11-15] and titanium oxides[15-19]. Of these, anatase TiO_2 is attractive because of easy processing of nanoparticles and extensive knowledge regarding its intercalation properties versus lithium.[20–24]

The electrochemical properties of anatase TiO_2 versus Na offer an appealing working voltage of 0.8 V, and researchers have already demonstrated high-rate capability, suggesting potential use in commercial cells.[25-28] Optimising the electrochemical properties of anatase TiO_2 for use in sodium-ion batteries requires a comprehensive understanding of the sodium intercalation mechanism, but this is still unclear despite previous studies. To the best of our knowledge, early studies on the sodium storage mechanism of TiO_2 could not conclusively identify the phases involved during the sodiation/de-sodiation reactions. Kim *et al.* have proposed that the anatase framework is maintained during the sodium intercalation, *i.e.*, *via* a solid-solution mechanism.[16] Nevertheless, the ex-situ x-ray diffraction data published in support of this proposal did not show the main line of the tetragonal phase, which therefore cannot be conclusive. Subsequently, Wu *et al.*, performed in-situ diffraction analysis showing that anatase amorphizes during the first discharge, yielding an amorphous electrochemically-active Na_xTiO_2 phase.[28] Louvain *et al.* have further confirmed the formation of an amorphous Na_xTiO_2 like phase using operando Raman spectroscopy.[29] These studies point out the need to clarify the structure of the newly formed amorphous Na_xTiO_2 and to identify the sodium storage mechanism occurring in anatase .

To resolve the sodium storage mechanism occurring in anatase TiO_2, we have used electrochemical and chemical routes to prepare reduced compounds, for which we obtained structural insights by combining high-energy synchrotron-based total scattering measurements, high resolution HAADF-STEM, magnetic measurements, and DFT calculations. Our analysis shows that intercalation of Na into anatase TiO_2 proceeds by a different mechanism to Li intercalation. Where $LiTiO_2$ maintains the pattern of edge-sharing TiO_6 octahedra of the anatase structure[30], Na intercalation produces a rhombohedral R-3m structure, accompanied by a decrease of long-range order. We also find that further electrochemical cycling proceeds via a phase transition between an amorphous anatase-like TiO_2 phase and disordered layered-like Na_xTiO_2 phase.

Experimental section

Synthesis and characterizations. Hydroxyfluorinated anatase was prepared by solvothermal synthesis according to reference [31]. Pure anatase TiO_2 nanoparticles was obtained by thermal treatment at 450 ºC under air for 4 hours. Powder X-ray diffraction (XRD) analysis was carried out using a Rigaku Ultima IV X-ray diffractometer equipped with a Cu Kα radiation source (λ = 1.54059 Å). Transmission Electron Microscopy (TEM) analysis was performed using a JEM ARM200F FEG double aberration corrected microscope operated at 200 kV, equipped with CENTURIO EDX detector and GIF Quantum. The sample was prepared in a glove box by suspending the powder in methanol and deposited it on holey carbon Cu grid. Afterwards the grid was immediately transport inside the microscope.

Electrochemical measurements. Electrodes were prepared by thoroughly mixing 80 wt. % active material, 10 wt. % black acetylene as the conductive agent and 10 wt. % sodium carboxymethyl cellulose[32] (CMC) as the binder. Then, the mixture was dispersed into a diluted H_2O_2 aqueous solution (H_2O_2 : H_2O = 2.5 : 97.5 v/v %) and coated on an aluminum foil. The electrodes were dried at 80 °C under air for 6 hours and under primary vacuum for 12 hours. Sodium half cells were assembled inside a glove box filled with Ar by using sodium foil as the negative electrode. A solution of 1 M $NaPF_6$ dissolved in ethylene carbonate and diethyl carbonate (EC:DEC) was used as the electrolyte. A sandwich-like film composed of glass filter in the two sides and polyolefin in the middle wasused as the separator. The Na cells were cycled between 0.0–2.0 V at a current density of 25 mA g^{-1} using galvanostatic discharge–charge testers (TOSCAT-3100, Toyo System Co. Ltd.). For ex-situ measurements, the cells were stopped at different state of discharge/charge, opened in a glove box. The electrodes were washed with EC:DEC and DEC, scrapped from the current collector and stored in a glove box filled with Ar for further characterizations.

Synchrotron diffraction. Samples were loaded inside Kapton capillaries. Data were collected at the 11-ID-B beamline at the Advanced Photon Source at Argonne National Laboratory, using high energy X-rays (λ = 0.2128 Å) allowing access to high values of momentum transfer.[33,34] One-dimensional diffraction data were obtained by integrating the raw 2D total scattering data in Fit2D.[35] PDFs, G(r), were extracted from the background and Compton scattering corrected data following Fourier transformation using PDFgetX2.[36] The Q_{max} was 22 Å. The PDFs were subsequently modelled using PDFgui.[37]

Chemical sodiation was performed using sodium naphtalenide as reducing agent. Anatase TiO_2 nanoparticles (200 mg) were dispersed in 20 mL of THF. Naphtalene (0.5 g) and small pieces of Na metal (170 mg) were added to the mixture and stirred in a glove box during 6 days at room temperature. Finally, the reduced phase was washed with THF and dry under vacuum.

Magnetic properties. The magnetic susceptibility χ as a function of temperature was obtained from magnetic moment measurements performed by squid magnetometry with a MPMS-5T from Quantum Design. The data were collected upon warming from 5K to 290K in a 100 Oe applied magnetic field in zero-field-cooling (zfc) and field-cooling (fc) processes. A diamagnetic correction was applied to χ_{mol}. Additional isothermal magnetic moment measurements were made as a function of the applied magnetic field H. In order to avoid air exposure, the preparation of the sample was made in a glove box. About 0.1 g of the sample powder was set within a gelatine capsule.

Computational. Density functional theory (DFT) calculations were performed using the plane-wave code VASP[38,39] with valence electrons described by a plane-wave basis with a cutoff of 500 eV. Interactions between core and valence electrons were described with the PAW method[40], with cores of [Mg] for Ti, [He] for O, and [Ne] for Na. The calculations used the revised Perdew-Burke-Ernzerhof generalized gradient approximation PBEsol[41], supplemented with a Dudarev +*U* correction applied to the Ti *d* states (GGA+*U*). We used a value of $U_{Ti,d}$ = 4.2 eV, which has previously been used to model lithium intercalation in anatase TiO_2 and in TiO_2-B[42-44]. All calculations were spin-polarized.

To model dilute Na-intercalated anatase TiO_2 we considered a single interstitial Na ion in a 4×4×2 supercell (384 atoms). Optimised lattice parameters were obtained by performing a series of constant–volume calculations for a stoichiometric anatase Ti_4O_8 cell, with the resulting volume–energy data fitted to the Murnaghan equation of state. These calculations were considered geometry-optimized when all atomic forces were smaller than 0.01 eV $Å^{-1}$. This procedure gives zero-pressure lattice parameters of *a* = 3.8495 Å and *c* = 9.5966 Å. These calculations used a 2×2×2 Monkhorst-Pack *k*-point mesh.

To model the fully sodiated phase we considered two structures for stoichiometric $NaTiO_2$: the rhombohedral O3-type layered structure[45] (space group R-3m) identified in our experiments, as discussed below, and the tetragonal "$LiTiO_2$" structure (space group $I4_1/amd$) observed by Wagemaker *et al.* for Li-intercalated anatase nanoparticles.[44] To compare the intercalation behaviour for sodium versus lithium, we performed calculations on both structures for compositions of $NaTiO_2$ and $LiTiO_2$. Calculations for the rhombohedral layered structure used a primitive cell (12 atoms) and a 4×4×1 Monkhorst-Pack *k*-point mesh. Calculations for the tetragonal "$LiTiO_2$" structure used a 2×1×1 supercell and a 2×4×2 Monkhorst-Pack *k*-point mesh. In each case starting structures were taken from the literature,[30,45] and full volume and geometry optimisations were performed, with the same convergence criteria as for dilute Na_xTiO_2.

To calculate sodium and lithium intercalation energies, reference calculations for metallic Na and Li were performed for 2-atom cells, using the same convergence criteria as above, and with a 16×16×16 Monkhorst-Pack grid for *k*–space sampling.

Results and Discussion

Electrochemistry. The electrochemical reaction of anatase TiO_2 nanoparticles (20 nm) with sodium was investigated using galvanostatic discharge–charge experiments. Details about material synthesis, characterizations and electrode preparation and testing can be found in the experimental section and Supporting Information. **Figure 1** displays the galvanostatic discharge-charge curves of the anatase TiO_2 (20 nm) electorde in Na half-cell tested between 0–2 V at a current density of 10 mA g^{-1}.

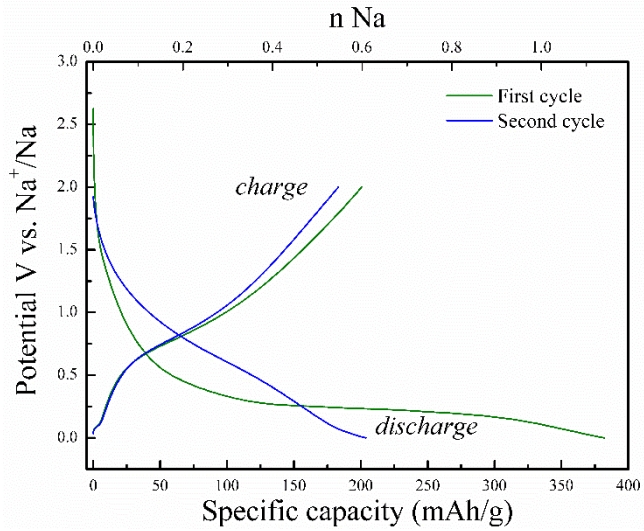

Figure 1. Galvanostatic discharge-charge curves of Na//TiO_2 cells. The cells were cycled at 25 mA.g^{-1}.

During the first discharge, the potential of the cell decreases rapidly from the open circuit voltage to 0.3 V, delivering a capacity of ~100 mAh/g, which corresponds to 0.3 Na^+ per formula unit, which should include the formation of passivation layer.[46,47] Afterwards, an irreversible plateau region was observed at ~0.2 V and delivered a capacity of ~280 mAh/g, corresponding to 0.84 Na^+ per TiO_2. The first discharge capacity was 380 mAh/g, exceeding the theoretical one, *i.e.* 335 mAh g^{-1} based on the Ti^{4+}/Ti^{3+} redox couple. The subsequent discharge-charge curves featuring a sloping profile and an average working voltage of ca. 0.8 V, differed from the first discharge indicating that an irreversible structural change occurring during the plateau region. Upon cycling, the Na-cell presents a reversible insertion/de-insertion of *ca.* 0.5 Na^+ per TiO_2. A capacity of 165 mAh/g was obtained after 50 cycles demonstrating that the activation of the electrode enabled reversible sodium uptake and release (**Figure S2 in Supporting Information**). Thus, the nature of the structural changes occurring during the first discharge is key to understand the reversible sodium storage mechanism.

Sodium storage mechanism. The structural changes associated with the electrochemical reaction with sodium upon the first discharge were investigated by high-energy x-ray diffraction. After full discharge, peaks from an anatase phase disappear and new broad Bragg peaks appear, indicating that sodium insertion induces a transition to a phase with decreased long-range order. The x-ray diffraction pattern of the discharged electrode was indexed with an O3-type Na_xTiO_2 rhombohedral structure (space group: R-3m) which captures the major features of the experimental data (**Figure S3**).[45] Note that the "O3" nomenclature referred to Delmas' notation indicating that the Na ions are octahedrally coordinated by oxygen and display a repetition period of three transition metal stacking along the c-axis.[48]

The structure of the electrochemically-sodiated Na_xTiO_2 phase was investigated through Pair Distribution Function (PDF) *G*(*r*), which was obtained from Fourier transformed

high-energy x–ray total scattering data. By providing real-space structural information that is independent of the long-range order, PDF is a powerful tool to investigate the structure of amorphous and nanostructured materials.[49] In keeping with x-ray diffraction analysis, the PDF was modeled using the O3-type Na_xTiO_2 rhombohedral type structure (space group: R-3m) which consists of a layered compound featuring sodium and titanium slabs with edge-shared $(Ti/Na)O_6$ octahedra. In its ordered form **(Inset Figure 2)**, Na and Ti occupy the 3a and 3b Wyckoff sites, respectively. Nevertheless, the observed transition from a tridimensional toward a layered like structure suggests a cation intermixing between the two slabs. Moreover, after the electrochemical sodiation of 0.3 Na^+ per TiO_2, PDF refinement of the partially sodiated electrode revealed minor structural changes **(Figure S4)** suggesting that the region observed prior to the plateau region arises from the decomposition of the electrolyte in agreement with another report.[25] Therefore, the first discharge corresponds to the reaction of 0.84 Na^+ per TiO_2. Accordingly, we considered a structural model involving non-stoichiometry and cationic inter-mixing. The PDF data was fitted as follows: (i) the rate occupancy of the 3a and 3b cation sites was refined, (ii) we considered an intermixing of Na and Ti atoms in Na/Ti slabs according to $(Na_xTi_y)_{3a}(Na_zTi_\alpha)_{3b}O_2$. The final refinement is shown in **Figure 2**. **Table 1** gathered the structural parameters obtained after the refinement. A good fit for the *r* region beyond 4 Å was obtained with a reliability factor of R_w = 26.5% (4 – 30 Å). Nevertheless, the PDF features in the local region, *i.e.* most notably from 1 to 4 Å but this extent up to 7 Å, cannot be well captured by the rhombohedral structure (R_w = 41.4% (1 – 30 Å), indicating strong local disorder due to cation inter-mixing. The refinement of the 3a site (Na slabs) indicates full occupancy and strong disorder with 43% of Na and 57% of Ti. The 3b site is partially occupied with 39% of Na and 39% of Ti. The chemical formula of the resulting phase is $(Na_{0.43}Ti_{0.57})_{3a}(\square_{0.22}Na_{0.39}Ti_{0.39})_{3b}O_2$ where □ refers to vacancy. Despite large standard deviation on the site occupancy, the number of Na deduced by the refinement agrees with the capacity obtained from the plateau region in **Figure 1**. As seen in **Table 1**, the unit cell parameters of $(Na_{0.43}Ti_{0.57})_{3a}(\square_{0.22}Na_{0.39}Ti_{0.39})_{3b}O_2$ are significantly lower than those of the ordered phase $NaTiO_2$. In particular, the c-parameters are 15.07 and 16.24 Å for $(Na_{0.43}Ti_{0.57})_{3a}(\square_{0.22}Na_{0.39}Ti_{0.39})_{3b}O_2$ and $NaTiO_2$, respectively. The strong contraction along the *c*-axis is consistent with the presence of high valence Ti^{IV} ions in the Na layers.[50]

To better understand the above structural analysis of the sodiated anatase, a scheme highlighting the structural relationship between the pristine tetragonal and sodiated rhombohedral phases is shown in **Figure 2** (bottom). Along the (100) direction, the filling of the interstitial sites by sodium produces a structure that can be viewed as a layered compound, where slabs are equally occupied by Ti and Na atoms. This layered-type structure appears to be highly distorted which explained the large standard deviation obtained on the site occupancy and the loss of long-range order.

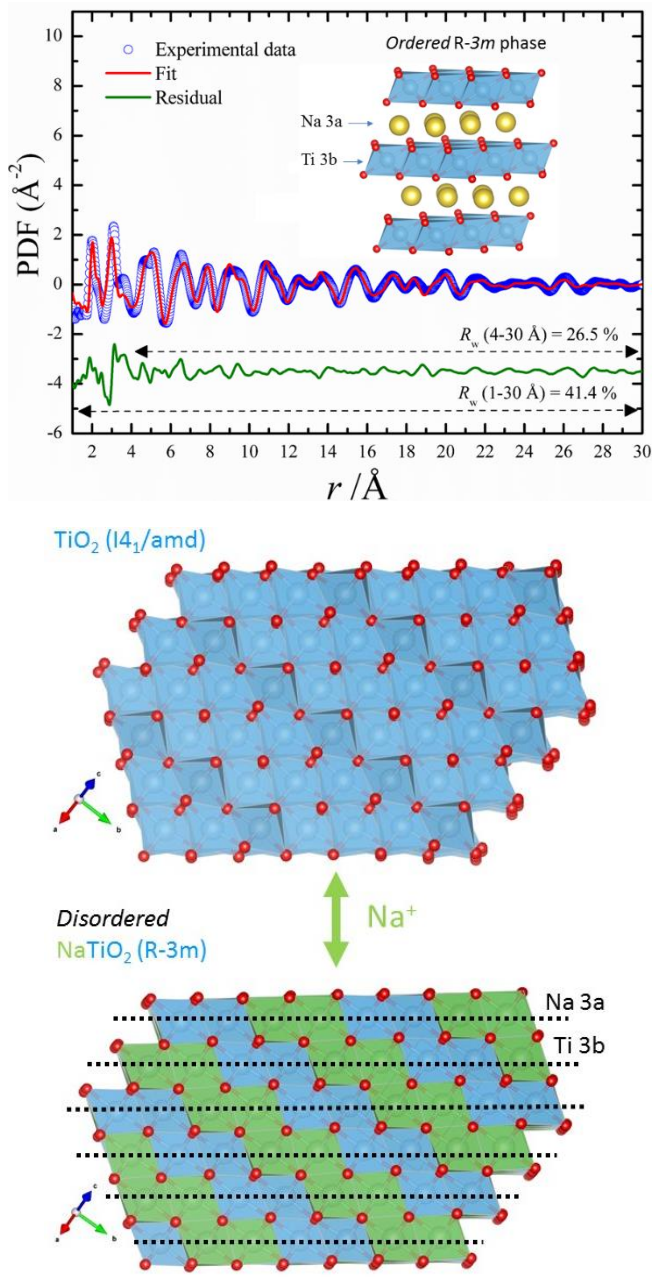

Figure 2. (Top) PDF refinement of the fully discharged electrode using an O3-type structure Na_xTiO_2 (space group: R-3m) model. Inset: structural representation of an ordered layered like $NaTiO_2$ phase. (Bottom) Structural relationship between the pristine tetragonal and sodiated rhombohedral phases, view is along the (100) direction.

Table 1. Structural parameters obtained by PDF refinement of the discharged electrode. For comparison purpose, the structural parameters of the ordered $NaTiO_2$ phase[45] were added.

	Discharged TiO_2	$NaTiO_2$ (ICSD # 85657)
a **[Å]**	2.989 (8)	3.05414 (4)
c **[Å]**	15.07 (9)	16.2412 (2)
V **[Å³]**	116.60	131.20
Site occupancy		
Na (3a)	0.43(25)	0.984(7)
Ti (3a)	0.57(25)	0.016(7)
Na (3b)	0.39(14)	0.016(7)
Ti (3b)	0.39(12)	0.984(7)
$d_{Ti/Na-O\ average}$	2.022	2.075
[Å]	2.305	2.390

De-insertion mechanism. To identify the mechanism enabling reversible electrochemical reactions with sodium, PDFs of the pristine, the fully discharged and fully charged electrodes were gathered in **Figure 3** with an emphasize on the short-range, *i.e.* $1 \leq r \leq 5$ Å, and long-range orders, *i.e.* *r*-values >5 Å.

Upon sodiation, the first peak at 1.941 Å (determined using Gaussian peak fitting), corresponding to Ti–O bonds, shifted to higher *r*-values with contributions at 1.937, 2.083 and 2.366 Å assigned to Ti^{4+}–O, Ti^{3+}–O and Na–O distances, respectively. This further supports that intercalation of sodium in anatase implies the Ti^{4+}/Ti^{3+} redox couple.

Upon de-sodiation, the peak associated with Na–O distance decreases in intensity indicating Na^+ de-insertion with a concomitant shift of the Ti–O bonds to lower *r*-value in agreement with the oxidation of Ti^{3+} to Ti^{4+}. Gaussian peak fitting of the Ti-O correlation indicates a remaining contribution of Ti^{3+}–O bonds emphasizing an incomplete sodium extraction which agrees with the charge capacity corresponding to 0.6 Na^+ per formula extracted from the discharged electrode **(Figure 1)**.

A comparison of the *r*-region >5 Å of the pristine and discharged/charged electrodes clearly demonstrates the dramatic loss of long-range order following the electrochemical reaction. While the pristine anatase appears to be effectively bulk, the ordered domains are reduced to 4 nm following sodium insertion. Strikingly, after sodium de-insertion, the length-scale further reduces to 2–3 nm (**Figure 3**). The anatase framework presents two types of Ti–Ti distances located at 3.04 Å (labeled A in Figure 3) and 3.79 Å (labeled B in Figure 3) corresponding to edge- and corner-sharing TiO_6 octahedra, respectively. Such features are partially recovered after de-sodiation indicating that the oxidized phase presents the short-range order of anatase. High-energy X-ray data of the charged sample showed a small peak which can be assigned to the (101) of the anatase type structure further supporting the recovery of the framework **(Figure S5).** Attempt to refine the PDF data of the charged electrode revealed that the recovered anatase is highly amorphous with a coherence length of less than 1 nm **(Figure S6)**.

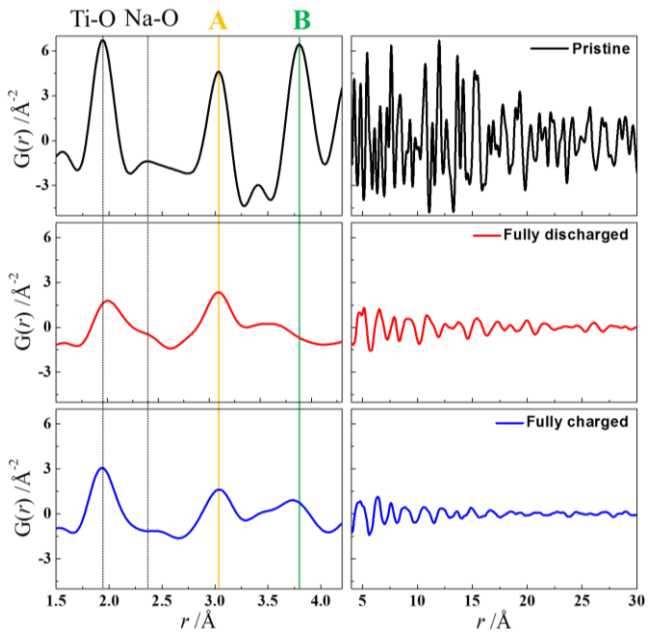

Figure 3. PDF profiles of the pristine (black), fully discharged (red) and fully charged (blue) electrodes. A and B refer to the interatomic distances of Ti–Na/Ti in edge-sharing and corner-sharing $(Ti/Na)O_6$ octahedra, respectively.

Based on our results, the following mechanism accounting for the sodium storage in anatase can be proposed. Upon sodium insertion, the anatase type structure is converted into a layered like phase accompanied by a dramatic loss of long-range order due to strong cationic inter-mixing between the Ti and Na slabs. The first discharge corresponded to an activation step yielding an electroactive phase. According to Wu *et al.*, the structural re-arrangement occurring during the first discharge suggests the release of O_2, as detected by *in-situ* chromatography.[28] After sodium de-intercalation, the structure can no longer be considered as a layered compound but transforms to a heavily disordered three-dimensional network with a similar local structure to anatase. Reversible sodium insertion/de-insertion is insured by these two phases. This phase transition is, however, characterized by a solid solution-like potential curve. This phenomenon can be explained by the amorphous nature of the two phases, which leads to a spectrum of voltage profiles for the phase transition, that produces a sloping curve similar to a solid solution mechanism.[22,51] It should be noted that solid solution-like voltage curve has been also observed in the case of a phase transition from a highly disordered amorphous $Na_3Fe_3(SO_4)_2(OH)_6$ towards crystallized $NaFe_3(SO_4)2(OH)_6$.[52]

Chemical sodiation. Although attempts to reduce micron-sized anatase particles using a chemical route failed,[45] it can be anticipated that decreasing the size of the particles will increase the sodium solubility. Following Wagemaker's works on the chemical reactivity of TiO_2 nanoparticles vs. Li,[53] we employed a chemical route to reduce TiO_2 nanoparticles using Na-Naphetlane as the reducing agent (see experimental method). The reaction was left for six

days to reach equilibrium conditions. **Figure 4** shows the x-ray diffraction powder pattern of the chemically reduced phase. The chemical sodiation induced a strong reduction of the crystallinity and similarly to the electrochemical route, a phase transition toward a Na_xTiO_2 like phase was observed. This result indicates that both electrochemical and chemical sodiation yielded Na_xTiO_2 type phase. Accordingly, the x-ray diffraction pattern was fitted using a rhombohedral structure and the following unit cell parameters were obtained a=3.05 and c= 14.60 Å. The *c* value indicates cationic inter-mixing in agreement with the three-dimensional pristine structure. Moreover, the lower *c*-value obtained by chemical sodiation indicates a larger amount of inserted sodium.

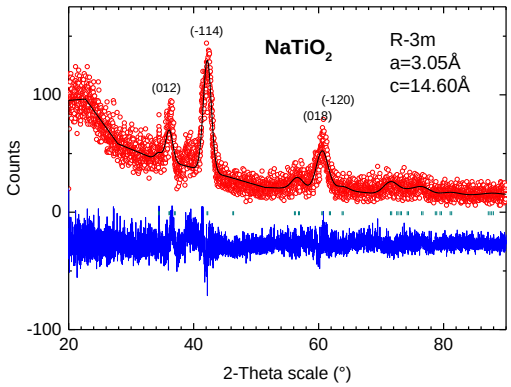

Figure 4. Le Bail profile refinement of the x-ray diffraction powder pattern of the reduced Na_xTiO_2 obtained by chemical sodiation.

Elemental analysis performed on reduced nanoparticles using energy-dispersive X-ray spectroscopy (EDX) yielded to a composition close to $Na_{0.9}TiO_2$. Elemental mapping on nanoparticles presented in **Figure 5a** shows a homogeneous distribution of all elements, which is further evidenced from the overlay color image **(Figure 5b)**. Bright field HRTEM image and corresponding FT pattern **(Figure 5c)** of a fragment of nanoparticle oriented along the *c*-axis revealed lattice plane separation of 0.54 nm corresponding to the d_{002} spacing of the rhombohedral Na_xTiO_2 phase, in agreement with XRD analysis. Deeper atomic insights were obtained using high resolution HAADF-STEM performed on a single nanoparticle viewed along the [001] rhombohedral direction **(Figure 6)**. A close inspection by high-resolution HAADF-STEM revealed non-homogeneity at the atomic level. Contrast in HAADF-STEM image is proportional to the thicknesses of the crystal and atomic number ($\sim Z^2$). There is clear evidence of Na(Ti) atomic columns contrast variation. Some columns appear very bright with respect to the surrounding ones, and can be attributed to Ti-rich (Z=22) columns (marked by white arrows in the Figure 8 inset). Moreover, the presence of black holes distributed over the nanoparticles (marked by red arrows head in Figure 8 inset) can be associated with vacancies thus concluding on similar structural arrangement adopted by the electrochemically and chemically reduced phases.

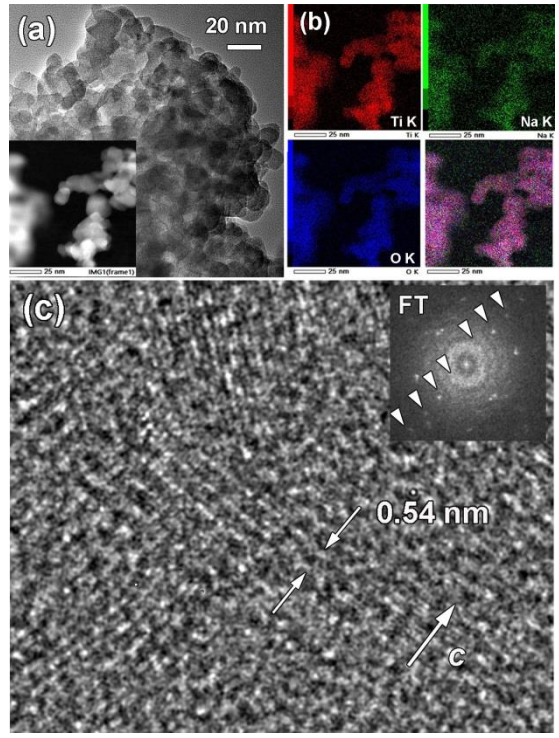

Figure 5. (a) Low magnification bright field TEM image of chemically reduced TiO_2 nanoparticles. Inset: HAADF-STEM image. (b) EDX elemental mapping for Ti K, Na K and O K. Overlay color image (right corner). (c) Bright field HRTEM image and corresponding FT pattern of fragment of nanoparticle oriented along the *c*-axis. Spots in the FT pattern depicted with white arrows correspond to the d_{002}=0.54 nm of the rhombohedral $Na_{0.9}TiO_2$ structure.

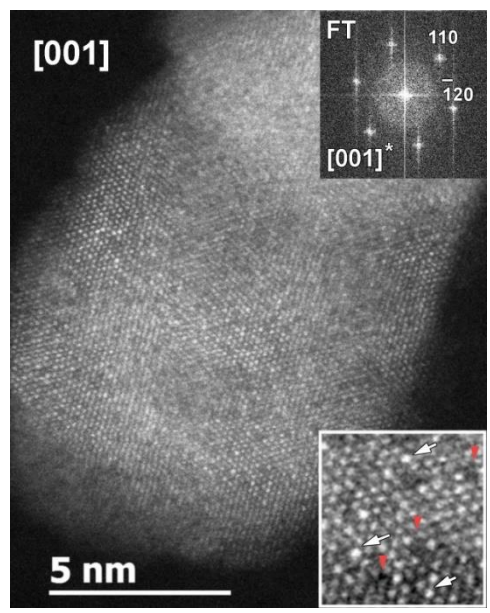

Figure 6. High-resolution HAADF-STEM image of Na_xTiO_2 nanoparticle viewing along 001 zone axis. Corresponding FT pattern is given as insert in right upper corner. Enlargement of HAADF-STEM image (right bottom corner) indicate the brightness variation of Na(Ti) columns: enhancement - by white and depletion – by red arrow heads.

Magnetic properties. The magnetic susceptibility measured as a function of the temperature of the sample chemically sodiated is shown in **Figure 7**. We noted that the small upturn in the $\chi(T)$ observed below ~50 K indicates a small Curie-Weiss paramagnetic component which could be attributed to a small amount of magnetic impurity, supported also by the slightly larger fc values. The $M(H)$ curve collected at 5 K (figure 9 inset) confirms this feature as M maximum values in 5 T reach only 0.01 μB/f.u. Overall, the $\chi(T)$ curve shows a rather T-independent χ from 50K to 290K for both zfc and fc curves with low χ values of about 10^{-3} emu.mol^{-1}. This result is consistent with Pauli paramagnetism resulting from the network of S=1/2 spins made by the majority Ti^{3+} in the disordered structure on which charge carriers are delocalized with three possible type of MO_6 with M=Ti, Na, and vacancy. The delocalized character ascribed to Ti–Ti distances is close to the Goodenough criterion.[54]

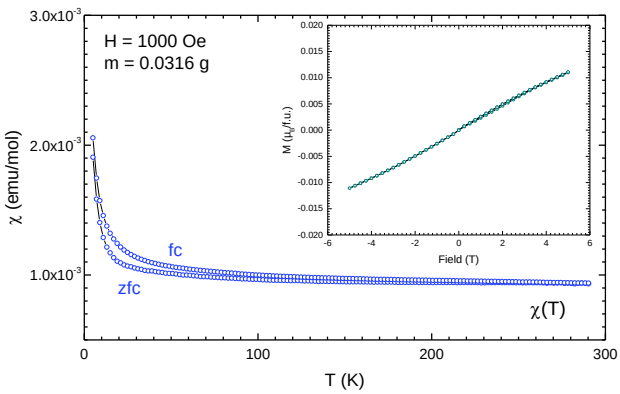

Figure 7. Susceptibility versus temperature for Na_xTiO_2 sample. Inset: M(H) curve at T=5K.

Clarke et *al*,[45,55] investigated the magnetic properties of ordered $NaTiO_2$ and $Na_{0.9}TiO_2$ samples. For a $NaTiO_2$ composition, they observed a magnetic transition at ~ 260 K ascribed to a monoclinic transition of the RT structure. Furthermore, the authors observed a similar transition for their $Na_{0.9}TiO_2$ sample, *i.e.* a composition very close to that of our chemically prepared material. The absence of the magnetic transition for the sample under study suggests that the structural transition observed in references[45,52] is responsible for the $\chi(T)$ transition. Moreover, both the pseudo-layered character of as prepared sample offering a large degree of ionic disorder as well as the smallness of the crystallites can explain the absence of the magnetic transition.

DFT calculations. To better understand the intercalation of sodium into anatase TiO_2, we performed DFT calculations for Na_xTiO_2 in the diluted limit and at the fully intercalated limit. To allow a direct comparison with the intercalation of lithium into anatase TiO_2, we also performed equivalent calculations for Li_xTiO_2.

To model intercalation in the diluted-limit, one Na or Li atom was placed at an octahedral interstitial site in a 4×4×2 $Ti_{128}O_{256}$ supercell, corresponding to x=0.008. For Na^+ intercalation, the Na^+ ion adopts a five-coordinate off-centre position (**Figure 8**), with average nearest Na–O separations of 2.13 Å, and a sixth Na–O distance of 3.28 Å. Constraining the Na ion to the centre of the interstitial octahedron increased the energy by 59 meV. In contrast, lithium does preferentially occupy the octahedron center, giving [4+2] coordination with average distances to the equatorial oxygen ions of 1.90 Å.[43] The calculated intercalation energy for Na, relative to metallic sodium, is -0.08 eV. This is significantly smaller (less negative) than the corresponding intercalation energy for Li, relative to metallic lithium, of -1.529 eV, and corresponds to a much smaller thermodynamic driving force for the initial intercalation of Na into anatase TiO_2 than for Li.

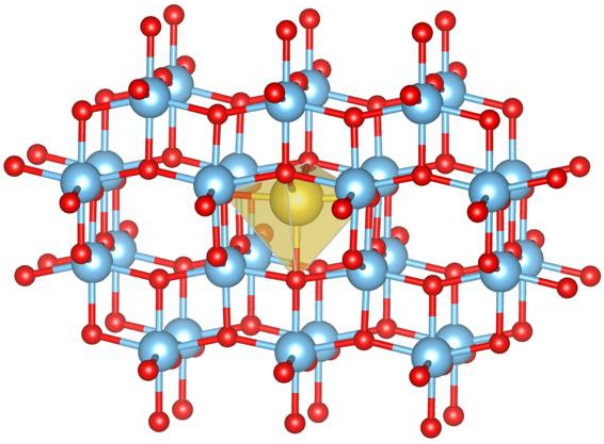

Figure 8. DFT optimized structure for Na in anatase TiO_2, showing the preferred off-centre coordination.

To model the fully sodiated limit, we performed DFT calculations on fully stoichiometric $NaTiO_2$ and $LiTiO_2$ (**Figure 9**). For Li_xTiO_2, the theoretical maximum of x=1 is only observed experimentally in sub-10 nm nanoparticles,[44,51] The reported $LiTiO_2$ structure is tetragonal ($I4_1$/amd), and preserves the edge-sharing between TiO_6 octahedra exhibited by pristine anatase TiO_2. In contrast, Na intercalation produces a rhombohedral R-3m phase. For our DFT calculations, we consider both $MTiO_2$ structures for M=Li and M=Na. For $NaTiO_2$, the rhombohedral structure gives an average intercalation energy of -1.247 eV Na^{-1}, and is more stable than the $LiTiO_2$ $I4_1$/amd structure by 0.272 eV per formula unit. In contrast, for $LiTiO_2$, we find the tetragonal $I4_1$/amd structure to be more stable by 0.110 eV per formula unit, with an average intercalation energy of -1.716 eV Li^{-1}.

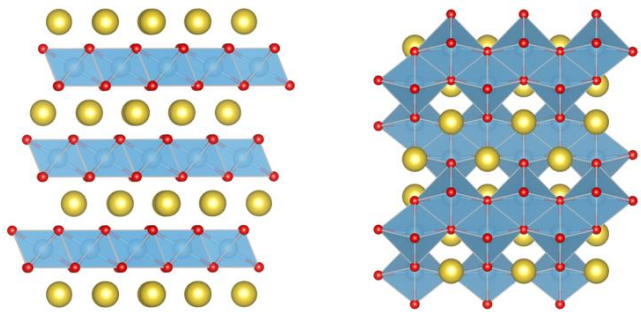

Figure 9. DFT optimized structures for stoichiometric $NaTiO_2$. Left panel: rhombohedral R-3m layered structure.[45] Right panel: tetragonal $I4_1/amd$ "$LiTiO_2$" structure.[30]

Conclusion

Here, we investigated the sodium intercalation mechanism in anatase TiO_2 emphasizing a complex process. During the first discharge, an irreversible plateau region was observed at ~0.2 V and enabled the electrode activation which can be further cycled with discharge-charge curves featuring a sloping profile and an average working voltage of *ca.* 0.8 V. Using PDF analysis, we identified the structural changes associated with the plateau region of the electrochemical profile demonstrating the stabilization of a rhombohedral phase Na_xTiO_2 showing high degree of disorder. The stabilization of such a structure was supported by DFT calculations which points out the structural difference between sodiated. The chemical formula deduced by PDF refinement led to $(Na_{0.43}Ti_{0.57})_{3a}(\square_{0.22}Na_{0.39}Ti_{0.39})_{3b}O_2$ where $\square$ refers to vacancy, highlighting the strong structural disorder due to cationic inter-mixing. Moreover, the presence of Ti cations in the Na slabs induced a contraction of the *c*-parameters as compared to the ordered phase $NaTiO_2$. PDF data of the charged electrode showed that the local structure of the anatase is recovered with short-range order of about 1 nm. Thus, the electrochemical process enabling the reversible sodiation/de-sodiation reactions implied the rhombohedral phase and an amorphous anatase phase yielding to a sloping composition-potential curves. Moreover, we showed that similarly to lithium, using chemical sodiation, downsizing the particle size increases the sodium solubility. Magnetic measurements performed on the reduced phase did not show any phase transition which is in contrast with the ordered phase.

ASSOCIATED CONTENT

Supporting Information. Detailed analysis such XRD pattern of the pristine, high-energy XRD of the discharged, charged electrode and PDF refinements. This material is available free of charge via the Internet at http://pubs.acs.org.

AUTHOR INFORMATION

Corresponding Author

* damien.dambournet@upmc.fr

Funding Sources

The research leading to these results has received funding from the People Programme (Marie Curie Actions) of the European Union's Seventh Framework Programme (FP7/2007-2013) under REA grant agreement n°[321879] (FLUOSYNES). Support from the Royal Society (UF130329) and EPSRC (EP/L000202 & EP/N004302/1).

ACKNOWLEDGMENT

This research used resources of the Advanced Photon Source, a U.S. Department of Energy (DOE) Office of Science User Facility operated for the DOE Office of Science by Argonne National Laboratory under Contract No. DE-AC02-06CH11357. B. J. M. acknowledges support from the Royal Society (UF130329). This work made use of the ARCHER UK National Supercomputing Service (http://www.archer.ac.uk), via the membership of the UK's HPC Materials Chemistry Consortium, which is funded by EPSRC (EP/L000202).

REFERENCES

(1) Dunn, B.; Kamath, H.; Tarascon, J.-M. Electrical Energy Storage for the Grid: A Battery of Choices. *Science* **2011**, *334*, 928–935.

(2) Larcher, D.; Tarascon, J.-M. Towards Greener and More Sustainable Batteries for Electrical Energy Storage. *Nat. Chem.* **2014**, *7*, 19–29.

(3) Yabuuchi, N.; Kubota, K.; Dahbi, M.; Komaba, S. Research Development on Sodium-Ion Batteries. *Chem. Rev.* **2014**, *114*, 11636–11682.

(4) Pan, H.; Hu, Y.-S.; Chen, L. Room-Temperature Stationary Sodium-Ion Batteries for Large-Scale Electric Energy Storage. *Energy Environ. Sci.* **2013**, *6*, 2338–2360.

(5) Kundu, D.; Talaie, E.; Duffort, V.; Nazar, L. F. The Emerging Chemistry of Sodium Ion Batteries for Electrochemical Energy Storage. *Angew. Chem. Int. Ed.* **2015**, *54*, 3431–3448.

(6) Rousse, G.; Arroyo-de Dompablo, M. E.; Senguttuvan, P.; Ponrouch, A.; Tarascon, J.-M.; Palacín, M. R. Rationalization of Intercalation Potential and Redox Mechanism for A2Ti3O7 (A = Li, Na). *Chem. Mater.* **2013**, *25*, 4946–4956.

(7) Colbow, K. M.; Dahn, J. R.; Haering, R. R. 4th International Meetings on Lithium BatteriesStructure and Electrochemistry of the Spinel Oxides LiTi2O4 and Li43Ti53O4. *J. Power Sources* **1989**, *26*, 397–402.

(8) Scharner, S.; Weppner, W.; Schmid-Beurmann, P. Evidence of Two-Phase Formation upon Lithium Insertion into the Li1.33Ti1.67O4 Spinel. *J. Electrochem. Soc.* **1999**, *146*, 857–861.

(9) Sun, Y.; Zhao, L.; Pan, H.; Lu, X.; Gu, L.; Hu, Y.-S.; Li, H.; Armand, M.; Ikuhara, Y.; Chen, L.; Huang, X. Direct Atomic-Scale Confirmation of Three-Phase Storage Mechanism in Li4Ti5O12 Anodes for Room-Temperature Sodium-Ion Batteries. *Nat. Commun.* **2013**, *4*, 1870.

(10) Senguttuvan, P.; Rousse, G.; Vezin, H.; Tarascon, J.-M.; Palacín, M. R. Titanium(III) Sulfate as New Negative Electrode for Sodium-Ion Batteries. *Chem. Mater.* **2013**, *25*, 2391–2393.

(11) Shirpour, M.; Cabana, J.; Doeff, M. New Materials Based on a Layered Sodium Titanate for Dual Electrochemical Na and Li Intercalation Systems. *Energy Environ. Sci.* **2013**, *6*, 2538–2547.

(12) Wang, Y.; Yu, X.; Xu, S.; Bai, J.; Xiao, R.; Hu, Y.-S.; Li, H.; Yang, X.-Q.; Chen, L.; Huang, X. A Zero-Strain Layered Metal Oxide as the Negative Electrode for Long-Life Sodium-

Ion Batteries. *Nat. Commun.* **2013**, *4*, 2365.
(13) Yu, H.; Ren, Y.; Xiao, D.; Guo, S.; Zhu, Y.; Qian, Y.; Gu, L.; Zhou, H. An Ultrastable Anode for Long-Life Room-Temperature Sodium-Ion Batteries. *Angew. Chem. Int. Ed.* **2014**, *53*, 8963–8969.
(14) Wu, D.; Li, X.; Xu, B.; Twu, N.; Liu, L.; Ceder, G. NaTiO2: A Layered Anode Material for Sodium-Ion Batteries. *Energy Environ. Sci.* **2014**, *8*, 195–202.
(15) Kim, K.-T.; Ali, G.; Chung, K. Y.; Yoon, C. S.; Yashiro, H.; Sun, Y.-K.; Lu, J.; Amine, K.; Myung, S.-T. Anatase Titania Nanorods as an Intercalation Anode Material for Rechargeable Sodium Batteries. *Nano Lett.* **2014**, *14*, 416–422.
(16) Xu, Y.; Lotfabad, E. M.; Wang, H.; Farbod, B.; Xu, Z.; Kohandehghan, A.; Mitlin, D. Nanocrystalline Anatase TiO2: A New Anode Material for Rechargeable Sodium Ion Batteries. *Chem. Commun.* **2013**, *49*, 8973–8975.
(17) Su, D.; Dou, S.; Wang, G. Anatase TiO2: Better Anode Material Than Amorphous and Rutile Phases of TiO2 for Na-Ion Batteries. *Chem. Mater.* **2015**, *27*, 6022–6029.
(18) Xiong, H.; Slater, M. D.; Balasubramanian, M.; Johnson, C. S.; Rajh, T. Amorphous TiO2 Nanotube Anode for Rechargeable Sodium Ion Batteries. *J. Phys. Chem. Lett.* **2011**, *2*, 2560–2565.
(19) Kavan, L. Lithium Insertion into TiO2. *J. Solid State Electrochem.* **2014**, *18*, 2297–2306.
(20) Ren, Y.; Hardwick, L. J.; Bruce, P. G. Lithium Intercalation into Mesoporous Anatase with an Ordered 3D Pore Structure. *Angew. Chem.* **2010**, *122*, 2624–2628.
(21) Sudant, G.; Baudrin, E.; Larcher, D.; Tarascon, J.-M. Electrochemical Lithium Reactivity with Nanotextured Anatase-Type TiO2. *J. Mater. Chem.* **2005**, *15*, 1263–1269.
(22) Wagemaker, M.; Mulder, F. M. Properties and Promises of Nanosized Insertion Materials for Li-Ion Batteries. *Acc. Chem. Res.* **2013**, *46*, 1206–1215.
(23) Shen, K.; Chen, H.; Klaver, F.; Mulder, F. M.; Wagemaker, M. Impact of Particle Size on the Non-Equilibrium Phase Transition of Lithium-Inserted Anatase TiO2. *Chem. Mater.* **2014**, *26*, 1608–1615.
(24) Wu, L.; Buchholz, D.; Bresser, D.; Gomes Chagas, L.; Passerini, S. Anatase TiO2 Nanoparticles for High Power Sodium-Ion Anodes. *J. Power Sources* **2014**, *251*, 379–385.
(25) Tahir, M. N.; Oschmann, B.; Buchholz, D.; Dou, X.; Lieberwirth, I.; Panthöfer, M.; Tremel, W.; Zentel, R.; Passerini, S. Extraordinary Performance of Carbon-Coated Anatase TiO_2 as Sodium-Ion Anode. *Adv. Energy Mater.* **2016**, 6, n/a – n/a.
(26) Ni, J.; Fu, S.; Wu, C.; Maier, J.; Yu, Y.; Li, L. Self-Supported Nanotube Arrays of Sulfur-Doped TiO2 Enabling Ultrastable and Robust Sodium Storage. *Adv. Mater.* **2016**, *28*, 2259–2265.
(27) Hwang, J.-Y.; Myung, S.-T.; Lee, J.-H.; Abouimrane, A.; Belharouak, I.; Sun, Y.-K. Ultrafast Sodium Storage in Anatase TiO2 Nanoparticles Embedded on Carbon Nanotubes. *Nano Energy* **2015**, *16*, 218–226.
(28) Wu, L.; Bresser, D.; Buchholz, D.; Giffin, G. A.; Castro, C. R.; Ochel, A.; Passerini, S. Unfolding the Mechanism of Sodium Insertion in Anatase TiO2 Nanoparticles. *Adv. Energy Mater.* **2015**, 5 (2), n/a – n/a.
(29) Louvain, N.; Henry, A.; Daenens, L.; Boury, B.; Stievano, L.; Monconduit, L. On the Electrochemical Encounter between Sodium and Mesoporous Anatase TiO2 as a Na-Ion Electrode. *CrystEngComm* **2016**, *18*, 4431–4437.
(30) Borghols, W. J. H.; Lützenkirchen-Hecht, D.; Haake, U.; van Eck, E. R. H.; Mulder, F. M.; Wagemaker, M. The Electronic Structure and Ionic Diffusion of Nanoscale LiTiO2 Anatase. *Phys. Chem. Chem. Phys.* **2009**, *11*, 5742–5748.
(31) Li, W.; Corradini, D.; Body, M.; Legein, C.; Salanne, M.; Ma, J.; Chapman, K. W.; Chupas, P. J.; Rollet, A.-L.; Julien, C.; Zhagib, K.; Duttine, M.; Demourgues, A.; Groult, H.; Dambournet, D. High Substitution Rate in TiO_2 Anatase Nanoparticles with Cationic Vacancies for Fast Lithium Storage. *Chem. Mat.* **2015**, *27*, 5014–5019.
(32) Dahbi, M.; Nakano, T.; Yabuuchi, N.; Ishikawa, T.; Kubota, K.; Fukunishi, M.; Shibahara, S.; Son, J.-Y.; Cui, Y.-T.; Oji, H.; Komaba, S. Sodium Carboxymethyl Cellulose as a Potential Binder for Hard-Carbon Negative Electrodes in Sodium-Ion Batteries. *Electrochem. Commun.* **2014**, *44*, 66–69.
(33) Chupas, P. J.; Qiu, X.; Hanson, J. C.; Lee, P. L.; Grey, C. P.; Billinge, S. J. L. Rapid-Acquisition Pair Distribution Function (RA-PDF) Analysis. *J. Appl. Crystallogr.* **2003**, *36*, 1342–1347.
(34) Chupas, P. J.; Chapman, K. W.; Lee, P. L. Applications of an Amorphous Silicon-Based Area Detector for High-Resolution, High-Sensitivity and Fast Time-Resolved Pair Distribution Function Measurements. *J. Appl. Crystallogr.* **2007**, *40*, 463–470.
(35) Hammersley, A. P.; Svensson, S. O.; Hanfland, M.; Fitch, A. N.; Hausermann, D. Two-Dimensional Detector Software: From Real Detector to Idealised Image or Two-Theta Scan. *High Pressure Res.* **1996**, *14*, 235–248.
(36) Qiu, X.; Thompson, J. W.; Billinge, S. J. L. PDFgetX2: A GUI-Driven Program to Obtain the Pair Distribution Function from X-Ray Powder Diffraction Data. *J. Appl. Cryst.* **2004**, *37*, 678–678.
(37) Farrow, C. L.; Juhas, P.; Liu, J. W.; Bryndin, D.; Božin, E. S.; Bloch, J.; Proffen, T.; Billinge, S. J. L. PDFfit2 and PDFgui: Computer Programs for Studying Nanostructure in Crystals. *J. Phys.: Condens. Matter* **2007**, *19*, 335219.
(38) Kresse, G.; Hafner, J. Norm-Conserving and Ultrasoft Pseudopotentials for First-Row and Transition Elements. *J. Phys.: Condens. Matter* **1994**, *6*, 8245.
(39) Kresse, G.; Furthmüller, J. Efficiency of Ab-Initio Total Energy Calculations for Metals and Semiconductors Using a Plane-Wave Basis Set. *Comput. Mater. Sci.* **1996**, *6*, 15–50.
(40) Kresse, G.; Joubert, D. From Ultrasoft Pseudopotentials to the Projector Augmented-Wave Method. *Phys. Rev. B* **1999**, *59*, 1758–1775.
(41) Perdew, J. P.; Ruzsinszky, A.; Csonka, G. I.; Vydrov, O. A.; Scuseria, G. E.; Constantin, L. A.; Zhou, X.; Burke, K. Restoring the Density-Gradient Expansion for Exchange in Solids and Surfaces. *Phys. Rev. Lett.* **2008**, *100*, 136406.
(42) Morgan, B. J.; Watson, G. W. GGA+U Description of Lithium Intercalation into Anatase TiO_2. *Phys. Rev. B* **2010**, *82*, 144119.
(43) Morgan, B. J.; Watson, G. W. Role of Lithium Ordering in the LixTiO2 Anatase → Titanate Phase Transition. *J. Phys. Chem. Lett.* **2011**, *2*, 1657–1661.
(44) Morgan, B. J.; Madden, P. A. Lithium Intercalation into TiO_2(B): A Comparison of LDA, GGA, and GGA+*U* Density Functional Calculations. *Phys. Rev. B* **2012**, *86*, 035147.
(45) Clarke, S. J.; Fowkes, A. J.; Harrison, A.; Ibberson, R. M.; Rosseinsky, M. J. Synthesis, Structure, and Magnetic Properties of $NaTiO_2$. *Chem. Mater.* **1998**, *10*, 372–384.
(46) Komaba, S.; Murata, W.; Ishikawa, T.; Yabuuchi, N.; Ozeki, T.; Nakayama, T.; Ogata, A.; Gotoh, K.; Fujiwara, K.

Electrochemical Na Insertion and Solid Electrolyte Interphase for Hard-Carbon Electrodes and Application to Na-Ion Batteries. *Adv. Funct. Mater.* **2011**, *21*, 3859–3867.
(47) Dahbi, M.; Nakano, T.; Yabuuchi, N.; Fujimura, S.; Chihara, K.; Kubota, K.; Son, J.-Y.; Cui, Y.-T.; Oji, H.; Komaba, S. Effect of Hexafluorophosphate and Fluoroethylene Carbonate on Electrochemical Performance and the Surface Layer of Hard Carbon for Sodium-Ion Batteries. *ChemElectroChem* **2016**, *3*, 1856–1867.
(48) Delmas, C.; Fouassier, C.; Hagenmuller, P. Structural Classification and Properties of the Layered Oxides. *Physica B+C (Amsterdam)* **1980**, *99*, 81–85.
(49) Billinge, S. J. L.; Kanatzidis, M. G. Beyond Crystallography: The Study of Disorder, Nanocrystallinity and Crystallographically Challenged Materials with Pair Distribution Functions. *Chem. Comm.* **2004**, No. 7, 749.
(50) Maazaz, A.; Delmas, C.; Hagenmuller, P. A Study of the $NaxTiO_2$ System by Electrochemical Deintercalation. *J. Inclusion Phenom.* **1983**, *1*, 45–51.
(51) Van der Ven, A.; Wagemaker, M. Effect of Surface Energies and Nano-Particle Size Distribution on Open Circuit Voltage of Li-Electrodes. *Electrochem. Commun.* **2009**, *11*, 881–884.
(52) Gnanavel, M.; Lebedev, O. I.; Bazin, P.; Raveau, B.; Pralong, V. Reversible Transformation from Amorphouse Na3Fe3(SO4)2(OH)6 to Crystallized NaFe3(SO4)2(OH)6 Jarosite-Type Hydroxysulfate. *Solid State Ionics* **2015**, *278*, 38–42.
(53) Wagemaker, M.; Borghols, W. J. H.; Mulder, F. M. Large Impact of Particle Size on Insertion Reactions. A Case for Anatase LixTiO2. *J. Am. Chem. Soc.* **2007**, *129*, 4323–4327.
(54) Goodenough, J. B. *Magnetism and the Chemical Bond*; Interscience Publishers, 1963.
(55) Clarke, S. J.; Duggan, A. C.; Fowkes, A. J.; Harrison, A.; Ibberson, R. M.; Rosseinsky, M. J. Single-Phase Na1.0TiO2: Solid-State Synthesis and Characterisation by High-Resolution Powder Diffraction. *Chem. Commun.* **1996**, No. 3, 409–410.
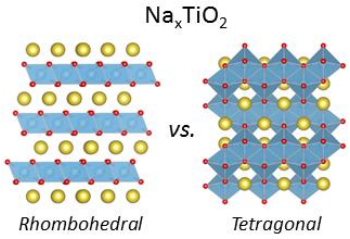
Authors are required to submit a graphic entry for the Table of Contents (TOC) that, in conjunction with the manuscript title, should give the reader a representative idea of one of the following: A key structure, reaction, equation, concept, or theorem, etc., that is discussed in the manuscript. Consult the journal's Instructions for Authors for TOC graphic specifications.